Research Article Vol. 42, No. 5 / May 2025 / Journal of the Optical Society of America A B379

Journal of the Optical Society of America A

OPTICS, IMAGE SCIENCE, AND VISION

Quantifying CIE alpha-opic signals in the indoor built environment

Samuel Ponting,[1,*] Ruth Kelly Waskett,[2] Manuel Spitschan,[3,4] and Hannah E. Smithson[1]

[1]Department of Experimental Psychology, University of Oxford, Oxford, UK
[2]Hoare Lea, London, UK
[3]Technical University of Munich, Munich, Germany
[4]Max Planck Institute of Biological Cybernetics, Tubingen, Germany
*samuel.ponting@pmb.ox.ac.uk

Received 8 November 2024; revised 7 February 2025; accepted 8 February 2025; posted 10 February 2025; published 14 March 2025

As humans spend more time in mixed-illuminant "built" environments, it is important to quantify how light in indoor spaces differs from naturalistic scenes. Previous studies have quantified light across many natural environments and shown regularities in the chromatic variation across different seasons, times of day, and weather patterns. This study measures light in a typical mixed-illuminant office space in the northern hemisphere (51.76°N, −1.27°W) and finds that it shares some regularities of chromatic variation with naturalistic scenes. In this dataset, such regularities are primarily conveyed through outdoor light entering through east- and north-facing windows and reflected by surfaces inside the office, rather than by light directly imaged through the north-facing window that was visible in the camera field-of-view. Built environments that combine natural daylight and artificial light to create mixed-illuminant spaces can share many of the statistical regularities that have been found in natural environments.

https://doi.org/10.1364/JOSAA.545151

1. INTRODUCTION

The chromatic properties of the lighting environments in which we find ourselves have a significant effect on our color vision, and this is attributed to processes of adaptation that optimize our visual systems to encode useful color information from our surroundings. As such, these optimizations are malleable and change over time as our environment changes, which in turn affects color perception [1–4]. The effects of adaptation to statistical regularities have been measured in infants as young as 4 months old [5], but long-lasting adaptation to different chromatic environments can yield significant changes to color vision throughout the lifetime [1]. A number of datasets recorded in natural scenes have sought to quantify typical lighting environments in different parts of the world, such as Japan, South Africa, and Canada, among others [6–10]. These datasets have demonstrated a number of reliably measured statistical regularities, both in the composition of individual scenes, and how these scenes change throughout the year due to seasonal variations in foliage, cloud coverage, and sun paths. This study seeks to characterize the available light in an example mixed-illuminant office environment and determine whether some of the statistical features quantified in natural environment recordings are reproduced in indoor environments where the natural world is reduced in its influence over the scene, and artificial lights and surfaces additionally play a role in determining our light exposure.

One example of a significant statistical regularity observed in natural scenes was shown by Webster *et al.* [9], who found significant chromatic differences when comparing the balance of light activating the long-wavelength cone population and light activating the medium-wavelength cone population ("L" and "M" hereafter) in "arid" and "lush" environments from images taken across different seasons in the Sayadhri Mountains (∼10°N, ∼77°E) in India and the Sierra Nevada Mountains (∼37°N, ∼3°W) in the USA. They demonstrated significantly lower ratios of L-activating light to M-activating light in lush environments, owing to the "greening" of foliage during spring or wet seasons. Webster *et al.* also found a number of other chromatic changes that occurred throughout the year, such as a shift in the distribution of colors in the MacLeod–Boynton chromaticity space—scenes examined in dry seasons showed a negative correlation between the S/(L + M) and L/(L + M) axes (where "S" refers to the activation of the short-wavelength cone population), which was not observed in wet seasons. While the aforementioned "greening" finding may be expected, it has significant implications for color appearance. Welbourne *et al.*

[11] examined unique yellow settings in a group of participants multiple times throughout the year, finding that unique yellow matches made in the winter (in York, UK 54°N, −1°W) had a higher long wavelength intensity than matches made in summer.

Other statistical regularities observed in natural environments have been linked to psychophysical results, such as those found by Vincent *et al.* [12], who showed L:M excitation ratio differences in the lightest and darkest regions of natural scenes depended on the seasonal characteristics of the scenes. Buck and DeLawyer [13] showed that participants, when adapted to achromatic backgrounds of different luminances, made different unique yellow settings. This suggests that the visual system may have different L:M adaptation states in different luminance levels, which may be the result of the kinds of variations in chromaticity across different luminance levels observed in natural scenes.

While the above examples provide the basis for the development of long-term adaptation states driven by changes in natural statistics, it may be important to consider whether these statistics are relevant in chromatic environments typical of the modern industrialized world. Wide-ranging surveys of American people's time budgets suggest many spend around 90% of their time indoors [14], and thus quantifying the chromatic distributions of typical indoor environments becomes an important research goal for evaluating present-day adaptation stimuli, as well as the effects these might have on color appearance. Indoor mixed illuminant scenes present an interesting chromatic environment, as they feature complex interplay between natural outdoor lighting visible through windows, indoor artificial lighting, and the many surfaces inside the indoor environment that are lit by a combination of the two. Some research, particularly that motivated by lighting design, has sought to quantify light in the so-called "built environments," though this often focuses on the non-visual effects of light in office spaces [15–17], rather than chromatic adaptation to indoor environments. Developments in our understanding of the non-visual effects of light, through the discovery of intrinsically photosensitive retinal ganglion cells (ipRGCs), have created significant research and commercial interest around "human centric lighting" [18], and while this has led to the use of some dynamic lighting systems that reduce blue light intensity in the afternoon [19], longer-term seasonal effects are not widely incorporated. Combining visual and non-visual approaches that consider these factors across different time scales to humans' "spectral diet" [20] may be a useful way to answer questions about the effect of the built environment on those who use it.

We sought to collect a physiologically relevant dataset of indoor images that would allow us to gain some insight as to whether indoor environments behave similarly to naturalistic scenes previously reported. Specifically, we sought to evaluate whether the aforementioned differences in chromatic distributions were observed in a mixed-illuminant indoor environment that combined static indoor lighting with dynamic natural light from multiple windows. We considered two main predictions that would be affirmed if the influence of daylight entering the scene through windows was sufficient to impart natural statistical regularities into the indoor environment. First, we predicted that the ratio of L-cone activating light to M-cone activating light will be lower in spring and summer months compared to autumn and winter, coinciding with the seasonal "greening" effect [9]. Second, we predicted that the regions of the scene with the highest luminance will feature lower ratios of L- vs. M-cone activating light during autumn and winter, though we might expect this effect to be in the opposite direction in spring and summer months [9].

2. METHODS

A. Data Specification

Data were collected using the Westboro Photonics WP690E-Circ Imaging circadiometer, controlled by the Westboro Photonics Photometrica software. The circadiometer's sensor generates 3388 × 2712 pixel maps using five filters that are calibrated to conform to the CIE S 026/E:2018 CIE System for Metrology of Optical Radiation for ipRGC-Influenced Responses to Light [21]. This CIE report defines a standard observer model for the five photoreceptor classes of the human visual system, including sensitivity curves for the S-, M-, and L-cones, as well as rods and ipRGCs. The term "alpha-opic" is used to identify the outputs of each of these receptors. Thus, each sample is comprised of five 3388 × 2712 photoreceptor maps of the alpha-opic radiances across space. Additionally, each photoreceptor map is the result of a high dynamic range (HDR) stack of up to five images, determined by the Photometrica software, which selects from a range of exposure times in order to prevent over-/under-exposure in each sample. The data values are then scaled to represent radiance in $W/sr/cm^2$.

B. Camera Location

The office space chosen for data collection was an open-plan office area on the second floor of New Radcliffe House in Oxford, UK (51.76°N, −1.27°W). The camera was positioned in front of a desktop computer workstation at a seated head height to mimic the point-of-view of an individual sitting at the computer workstation. The office area was freely used by members of the Oxford Perception Lab throughout the duration of the image capture schemes. Ethical approval for this was granted by Oxford's Medical Sciences Interdivisional Research Ethics Committee with approval reference R81269/RE001. From the point of view of the camera, the desk, keyboard, and workstation monitor are visible, along with other furniture inside the office space, such as other desks, monitors, chairs, and cupboards. A prominent north-facing window is visible in the scene on the far side of the office. Additionally, three east-facing windows were located to the right of the camera. While these were not captured in the camera's images, significant light entered the workspace from these windows. Notably, the lights used throughout the office space were motion-activated, switching on whenever motion was detected in the area around the office, regardless of the ambient light level. The availability of artificial light is therefore linked to the core working hours of the users of the office space (08:30–18:00) and decoupled from the availability of natural light. Throughout the data collection periods, the screen remained on, in order to mimic the additional light provided by computer use in the office. The light emitted from

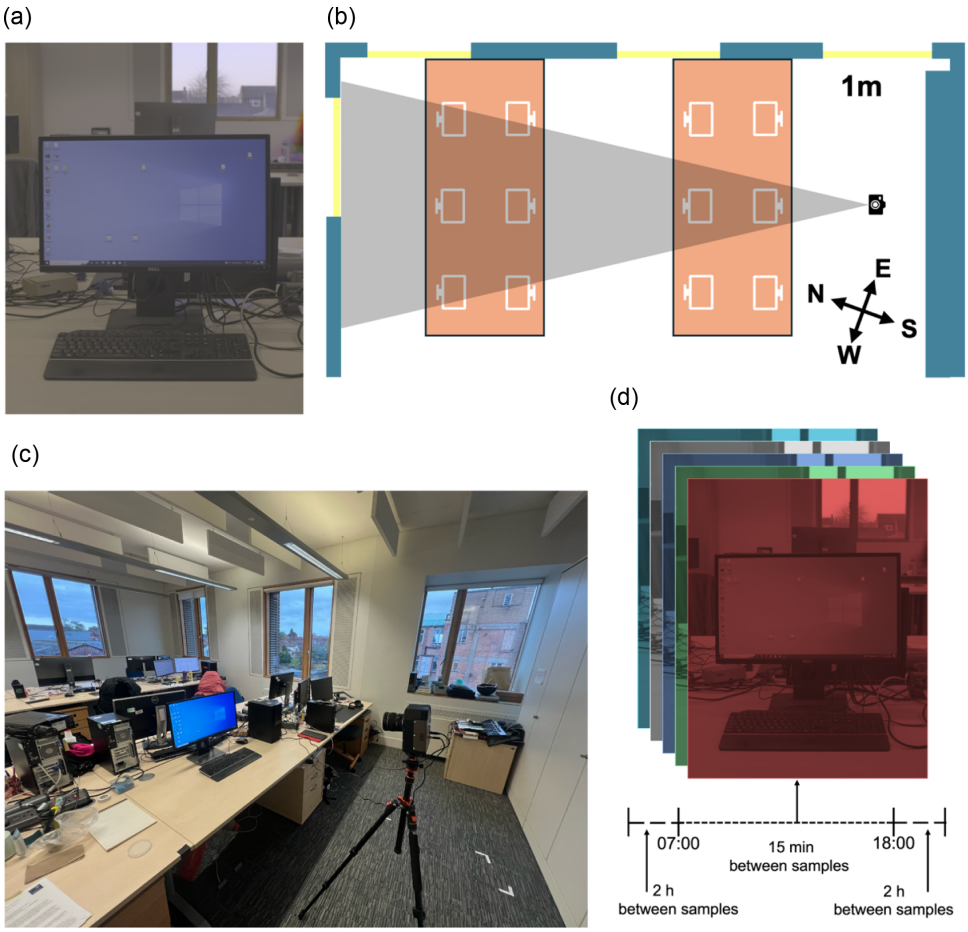

Fig. 1. Circadiometer setup information. (a) Recolorized image of the point of view of the circadiometer. (b) Bird's-eye schematic of the office space. Blue bars denote walls, and the yellow gaps in these walls represent windows. The orange blocks show the positions of the desks, with the computer workstations atop them. The camera icon shows the location of the camera. The shaded triangle approximates the area that is visible to the camera. The compass icon shows directions relative to the office space. (c) Side view of the location of the circadiometer. (d) Schematic of the data that are collected throughout the capture scheme, with 15 min sampling between 07:00 and 18:00, and 2 h sampling overnight. Each recording represents a five-layer map of each of the CIE alpha-opic radiances, each with a resolution of 3388 × 2712 pixels.

the screen remained constant throughout the data collection period. Figures 1(a)–1(c) contain images depicting the location and setup of the camera, as well as details about the surrounding office. Additional information about the artificial room illumination in the scene, information about the light emitted from the screen, and information about the terrain visible out of the windows is provided in Figs. S1, S2, and S3 in Supplement 1.

C. Capture Scheme

Figure 1(d) shows the capture scheme for a 24 h period within the seven day data collection period. Data captures were triggered automatically throughout the data collection periods every 15 min between 07:00 and 18:00 and every 2 h overnight. These timings were chosen to capture data at a high frequency during the early morning and "working day" hours and at a lower frequency outside of this time. Each HDR-stacked photoreceptor map was captured sequentially (in the order: S-cone, M-cone, L-cone, rhodopsin, and melanopsin). Each image capture took between 30 s and 2 min to complete, depending on the light intensity at the time of capture. This 24 h capture scheme was repeated over seven days, giving 329 time points, once in January 2023 and once in May 2024. These timings were selected in order to match the autumn/winter and spring/summer differences identified in previous literature demonstrating seasonal differences.

D. Data Validation

The circadiometer's output values were validated by comparing the values recorded in an image taken of an X-Rite ColorChecker in a Judge QC lightbox to measurements made by a PR-670 spectroradiometer of the same test patches in the same light setup. For each circadiometer filter, this validation check confirmed the linearity and appropriate spectral filtering of circadiometer outputs.

E. Data Analysis

To split the images into data-derived regions, a spatial principal component analysis (PCA) was performed on each dataset

individually. Each timepoint in the dataset was spatially downsampled by a factor of four before the PCA was conducted to reduce the number of variables in the analysis. Each downsampled pixel location was then treated as an independent variable, and each timepoint within the season as a separate observation of each of the variables. The PCA was conducted on log-transformed data, as this provided a more reliable and interpretable result. K-means clustering was applied to the resultant PCA scores, with a prior K value of three. Three was selected for the prior K value as it corresponds to three kinds of regions within the scene—the window, which provides a direct view of natural light, the indoor region, which reflects light emitted by the indoor artificial lights as well as the natural light let in by the window, and the screen, which itself emitted light throughout the duration of the data capture periods.

In order to evaluate the chromatic characteristics of the images, spectral statistics were calculated using L-cone, M-cone, S-cone, and melanopic activation maps. Scaling coefficients (0.689903 and 0.348322) were applied to L- and M-cone activations, respectively. This rescales the summation of L- and M-cone activations to the luminous efficiency function, $V(\lambda)$ [22]. No scale factor was used for S-cone and melanopsin activation maps. In addition to calculating the luminance, defined as $(L + M) * 683.002$, we calculated the chromaticity statistics for each pixel—$L/(L + M)$, $S/(L + M)$ and $I/(L + M)$, where L and M refer to the scaled L- and M-cone activation maps, and S and I refer to the unscaled S-cone and melanopsin activation maps.

When comparing these statistics, only data collected between sunrise and sunset for each dataset (so-called "daytime hours") were considered as the nighttime samples had low light levels and were therefore noisy. Within the January dataset, sunrise shifted from 08:01 to 07:54, and sunset shifted from 16:30 to 16:40. Within the May dataset, sunrise shifted from 05:00 to 04:54, and sunset shifted from 21:03 to 21:11. Core office hours remained between 08:30 and 18:00 throughout both datasets. Luminance-weighted chromatic statistics were also calculated to weigh chromaticity information by a measure of intensity to better capture the light energy contributing to adaptation.

Additionally, to analyze the rod data, we calculated the proportion of the scene intense enough to fully saturate the rods. To do this, we modeled pupil size using the average luminance across the scene and replication of Watson and Yellott's pupil response model [23,24]. We then downsampled the image dataset to match the acuity limit of the rods at 6.5 cycles per degree [25], then scaled scotopic luminance values by pupil area, and then by the peak scotopic efficiency of 1700 lm/W to find scotopic trolands. We used a threshold of 3000 scotopic trolands to determine the saturation cutoff [26,27]. We then calculated the proportion of saturated pixel locations over the time series of data collection.

Finally, we analyzed the indoor region more closely to identify the patterns that arise from the complex interplay of light across different surfaces. To do this, we calculated the correlations between luminance and the stated chromatic statistics across pixels within the indoor region over time. Additionally, the time series of luminance variation in each pixel location was fitted with a sinusoidal function in order to compare phase deviations between the indoor region and the window. The cosine fitting model was given a fixed periodicity corresponding to the 24 h diurnal cycle, fitting amplitude and phase in order to find the strength and delay on the 24 h variation in each pixel location.

3. RESULTS

A. Seasonal Variation

Figure 2 shows the results of the PCA and K-means clustering. Figures 2(a) and 2(d) show the amount of variance explained by each principal component for the January and May datasets, respectively. In both PCAs, the first principal component explains around 80% of the variance. In the January PCA, one additional component contributes more than 10% variance and, in the May PCA, there are two components both contributing more than 5% variance. Figures 2(b) and 2(e) show the distribution of pixels in the scene according to their scores on principal components 1 and 2. Figures 2(c) and 2(f) show the K-means clusters replotted onto the original scene. Both K-means classifications segment the scene into three regions broadly characterized by the "screen" (green), "indoor" (yellow), and "window" (purple) regions. Notably, the two classifications differ in their categorization of some pixels on the desk—being clustered with other "indoor" surfaces in January, but with the "window" pixels in May. Subsequent analysis (described in Supplement 1) revealed that this was the result of the changes in the sun path, where highly directional sunlight causes bright reflections from the desk.

Figure 3 shows chromatic statistics across daytime images in both seasonal datasets. Row 1 [Figs. 3(a)–3(c)] denotes $L/(L + M)$ statistics, row 2 [Figs. 3(d)–3(f)] denotes $I/(L + M)$ statistics, and row 3 [Figs. 3(g)–3(i)] denotes $S/(L + M)$ statistics, each plotted as a function of luminance. Within each figure, the January dataset is plotted in blue, and the May dataset in yellow. Each column relates to a spatial averaging of the data—data in column 1 are averaged across the whole image, data in column 2 are averaged only over the window region, and data in column 3 are averaged only across the indoor region. The curves to the right of each scatter plot and at the top of each column show the kernel-smoothed distributions of the data for each variable in each plot. The darkened bars denote the means for each distribution. For example, the datapoints in the middle column are calculated by averaging across the window, with each datapoint corresponding to a different point in time. Equally, the whole image column features statistics averaged across the indoor, window, and screen regions. Thus, the lowest luminance observed across the whole image is higher than that observed only in the window, as a result of the constant light emitted by the screen, incorporated into the whole image mean but not the window mean. The whole-image analysis (column 1) shows that datapoints from the May dataset have lower $L/(L + M)$ values and higher $I/(L + M)$ and $S/(L + M)$ values. Conversely, the window analysis (column 2) shows minimal seasonal differences in the window region. Notably, the whole image and indoor regions feature a small number of May datapoints with significantly higher luminances than the rest of the data. These datapoints—that appear above 450 cd/m^2 in the whole image data and above 200 cd/m^2 in the indoor data—all occur shortly after sunrise, before 09:00.

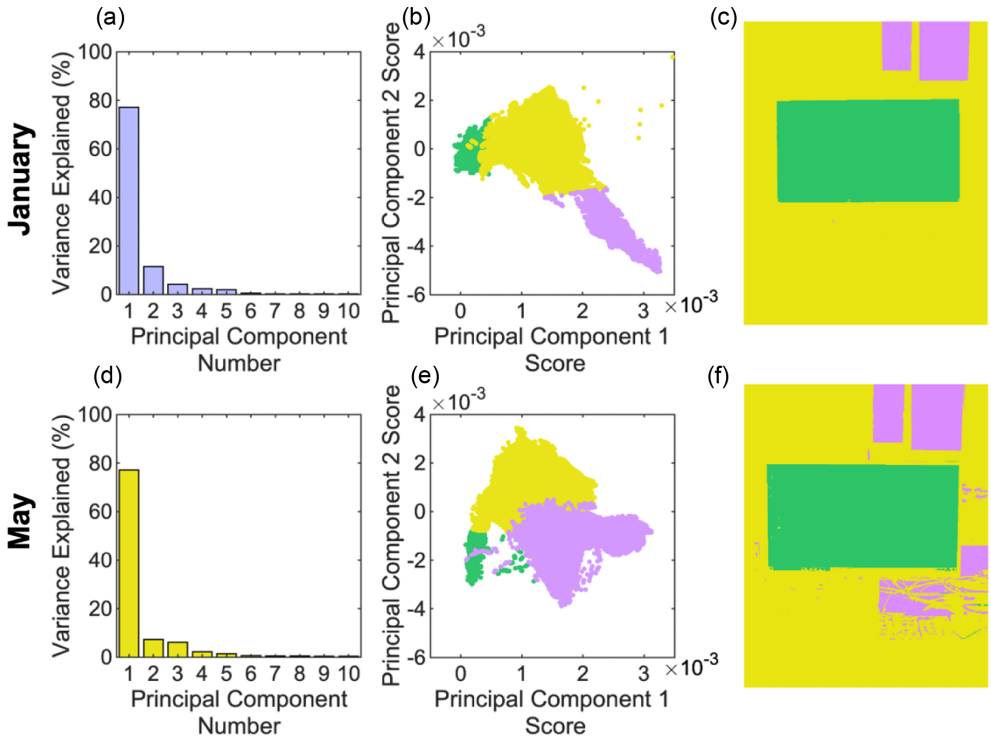

Fig. 2. PCA and K-means results. (a) and (d) The amount of variance explained by each principal component for the January and May datasets, respectively. (b) and (e) The distribution of pixel weightings for principal components 1 and 2, with colors reflecting the K-means clusters. (c) and (f) Clusters plotted back onto their position in the original scene.

The parametric Kruskal–Wallis test was used to compare each of these variables across the two seasonal datasets, as the presented data are not normally distributed. Results are shown in Table 1. Signs in Table 1 denote the direction of significant differences where they exist, such that "+" signs mean that a given region-statistic pair was higher in May than in January, and "−" signs mean that the region-statistic pair was lower in May. Significant differences were found across all statistics when the images were averaged as a whole. Where window region differences were found between the two seasons, they were significantly smaller, and no significant difference was found in the L/(L + M) statistic. The indoor region also showed significant differences between L/(L + M), I/(L + M), and luminance statistics, though not in S/(L + M).

To ensure that the differences in pixel location categorization did not significantly influence our comparisons of the January and May datasets, we conducted the presented statistical tests on data grouped into these clusters, as well as manually defined "window," "indoor," and "screen" regions, finding no difference in the season- and region-based effects. We additionally calculated luminance-weighted statistics for each region and season and conducted similar statistical testing. This is presented in Fig. S4 and Table S1 in Supplement 1.

Figure 4 shows L/(L + M) differences between indoor and window regions at the same time point. A positive difference means that the window region has a higher L/(L + M) value than the indoor region. January data are shown in blue and May data are shown in yellow. Figure 4 shows that for most of the May dataset, L/(L + M) is increased in the window region compared to the indoor region; however, the January dataset is bimodal, with some of the differences being positive and some negative, though the group with negative differences is larger than the group with positive differences. This bimodality is associated with weather effects (see Fig. S5 in Supplement 1, and further discussions below).

Figure 5 shows the percentage of the scene in which rods are saturated over time. The data show a consistent peak at around 6% of the scene throughout the January dataset. An example image from January demonstrates that this reflects the outdoor region of the scene being almost entirely rod-saturated, with no rod saturation occurring in the indoor portion of the scene. In May, there are persistent fluctuations above this level; an example image from May 28 shows that around 10% of the scene is rod-saturated. In addition to the window region, parts of the desk are also rod-saturated. This is the result of increased directional sunlight in the May dataset, which leads to bright reflections as the angle of direct sunlight approaches the surface normals of objects within the scene. Further examples show that on three occasions in the May dataset, the rod-saturation percentage spikes at around 26%, each time at 07:00. In these cases, the desk and some parts of the south-facing wall become rod-saturated, further demonstrating the effects of directional sunlight entering the scene.

B. Weather Variation

Figure 6 shows chromaticity plots for daytime samples across each season, averaged across the whole image, and the indoor and window regions. In each case, the data appears split into two groupings. A K-means (K = 2) clustering was used to classify

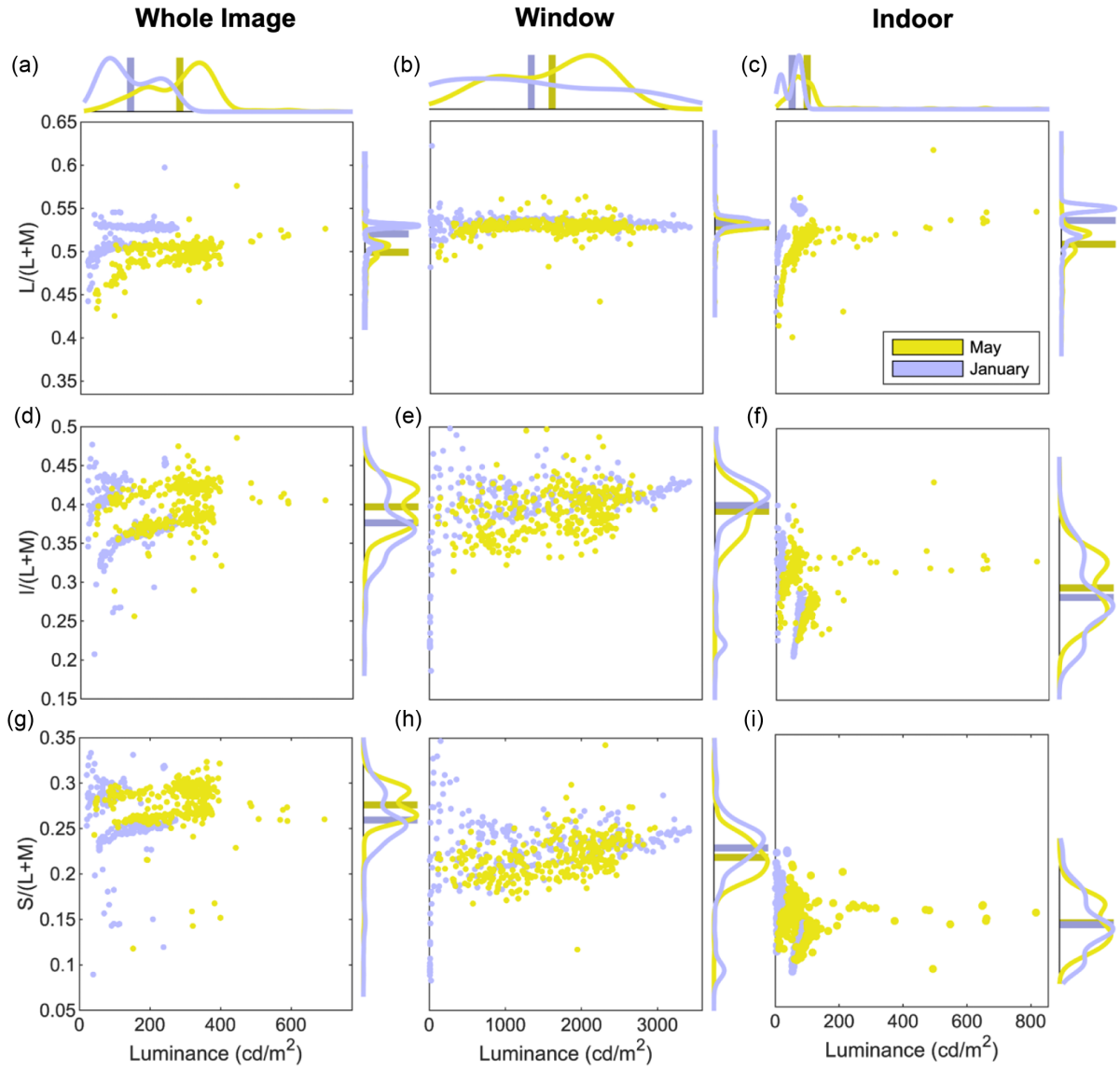

Fig. 3. Scatter plots and histograms for mean chromatic and luminance values across different regions comparing January and May datasets. January data are shown in blue, and May data in yellow. Each subplot shows a scatter plot and two kernel-smoothed histograms showing the distribution of each variable. Darkened bars on the histograms denote the mean for each variable. The left column shows the whole image data, the middle column shows the window region data, and the right column shows the indoor region data. The top row shows L/(L + M) statistics, the middle row shows I/(L + M) statistics, and the bottom row shows S/(L + M) statistics.

Table 1. Chromaticity Kruskal–Wallis Test Statistics for Seasonal Differences

		Luminance	$L/(L+M)$	$I/(L+M)$	$S/(L+M)$
Whole Image	χ^2	257.76+	24.55−	44.11+	59.89+
	p	**< 0.001**	**< 0.001**	**< 0.001**	**< 0.001**
Window	χ^2	30.21+	1.77	11.14−	6.25−
	p	**< 0.001**	0.184	**0.001**	**0.012**
Indoor	χ^2	153.14+	15.57−	4.56+	0.24
	p	**< 0.001**	**< 0.001**	**0.033**	0.621

these groupings, and the data are colorized to reflect them. The differences in these groups are characterized by a shift in both L/(L + M) and S/(L + M), such that the "orange" grouping have a lower S/(L + M) ratio and a higher L/(L + M) ratio, meaning they have less short-wavelength light and more long-wavelength light. Notably, data in the orange grouping, which make up the larger proportion of data across all conditions, have different relationships in January and May. In January, the data in this group have a negative slope, while the data in May show no obvious slope. Whole image data are significantly higher in S/(L + M) than the two region-based calculations, as the screen, which is omitted in the region-based calculations, emitted predominantly blue light.

Figure 7 is a timeseries plot showing the classification of samples over time, according to the K-means clustering of L/(L + M) versus S/(L + M) data presented in Fig. 6. Thus, daytime timepoints appear either orange or teal, and nighttime timepoints appear gray. Each row corresponds to the clustering within a particular season–region combination. While almost

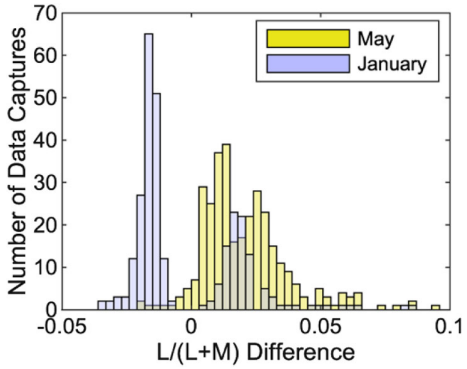

Fig. 4. Difference in L/(L + M) statistic between window and indoor regions within time points. Positive differences denote that L/(L + M) was higher in the window region. January data are shown in blue, and May data are shown in yellow.

all days in this time series contain both orange and teal times, the days can be categorized by their predominant grouping—January features five predominantly "orange" days and two "teal" days, while May features four "orange" days and three "teal" days. Notably, the teal grouping appears consistently at dawn and dusk on "orange" days. The classifications between groups are largely consistent across regions.

To investigate what might underlie the chromatic change between the different days, we investigated historical weather data for Oxford during the capture periods. Weather data were accessed at [28], where weather data are provided by CustomWeather, who report data from weather stations run by the World Meteorological Organization (WMO). Nearby weather reports suggest that throughout both of our dataset capture periods, days classified into the orange group featured some direct sunlight throughout the day. However, the days largely identified as teal had no recorded period of direct sunlight, often being characterized by "fog," or "overcast." This suggests that the earlier classification of days into "orange" and "teal" groups

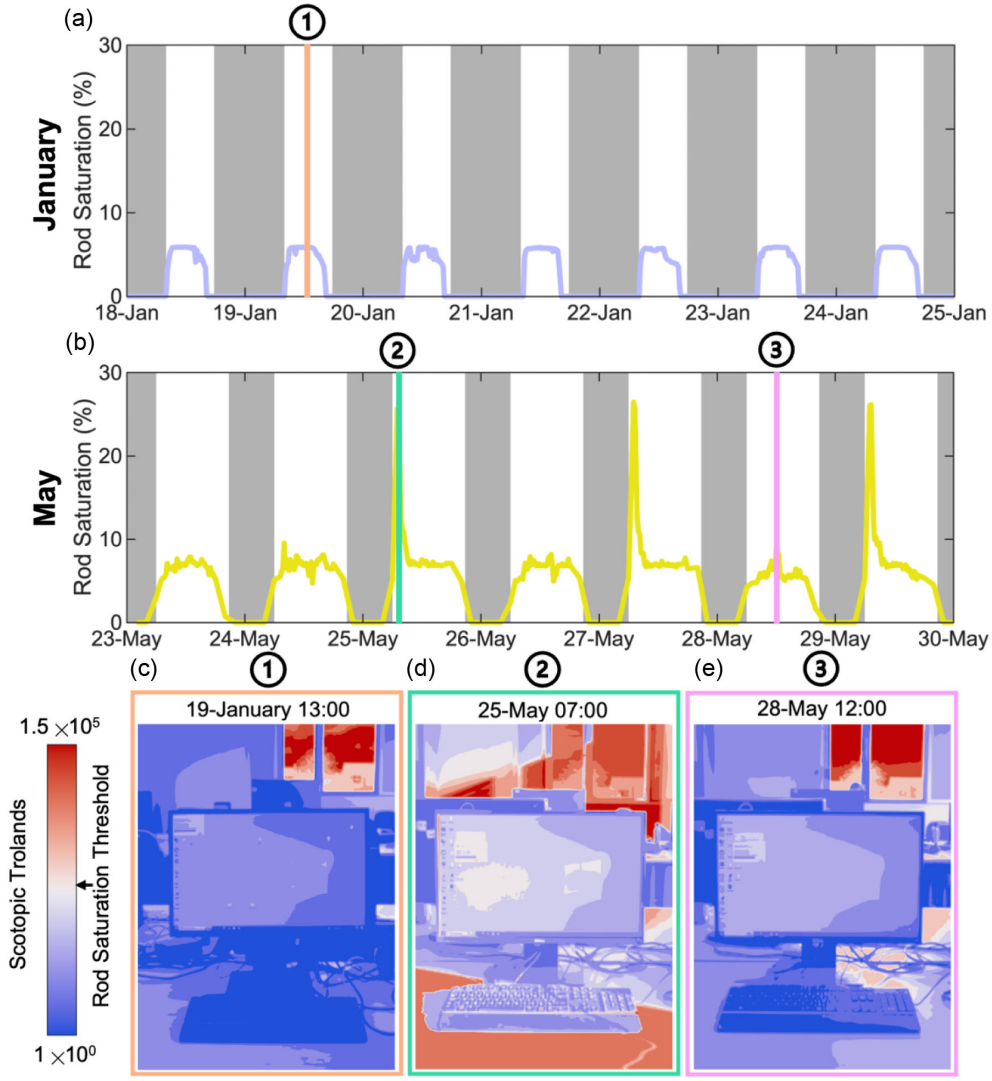

Fig. 5. Timeseries plots showing the percentage of the scene that saturates the rods over time in January (top row) and May (second row). Shaded time periods show the time between dusk and dawn. The bottom row shows contour plots of example time points from each of the datasets. In these schematics, red regions show where rod saturation has occurred and blue regions show where the scotopic troland level is below the saturation threshold.

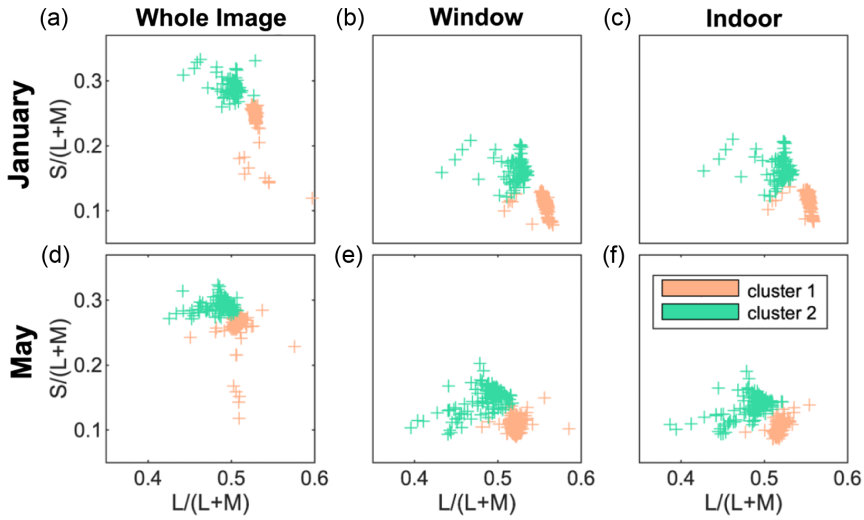

Fig. 6. Chromaticity plots for daytime samples across January (top row) and May (bottom row), averaged across the whole image, the indoor region, and the window region (columns). Data are colored by a K-means clustering.

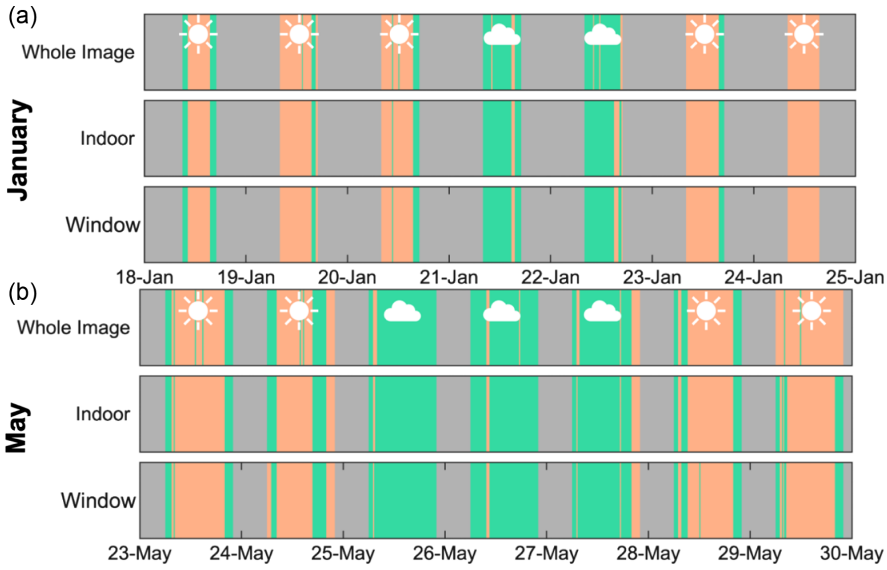

Fig. 7. Timeseries plots where timepoints are color-coded by the K-means cluster classification, based on the subplots in Fig. 5. Each row corresponds to a different season–region combination, with the top three rows corresponding to the whole image, indoor, and window region classifications for the January dataset, while the bottom three rows correspond to the May dataset. The gray shading appears before sunrise and after sunset. White weather icons denote the weather grouping for each day.

presented in Fig. 6 corresponds to "sunny" and "overcast" days, respectively.

Additional analysis of weather effects has been included in Supplement 1. First, we present analysis of the change in strength of the correlations between S-cone and melanopsin signals throughout each dataset, and across weather conditions (see Fig. S9). These two photoreceptor populations provide antagonistic signals to pupil control [29], and so their decorrelation in natural scenes is of physiological interest. Second, we analyze the correlation between luminance and various chromatic statistics across pixels within the indoor region, again across each dataset and weather condition (see Fig. S10).

C. Directional Variation

The direct sunlight that enters the office appears to be a major source of chromatic changes but is highly time-dependent as the position of the sun changes throughout the capture periods. To capture this variation, we have investigated luminance as a function of time for each pixel, fitting a cosine model for each luminance profile. This allows us to determine the size of changes in the magnitude and phase of diurnal luminance variation across parts of the scene. Figure 8 shows relative phase delay histograms for pixels in the window and indoor regions, corresponding to the distribution of phases from the cosine fits to each pixel. Data from the January dataset are shown in blue,

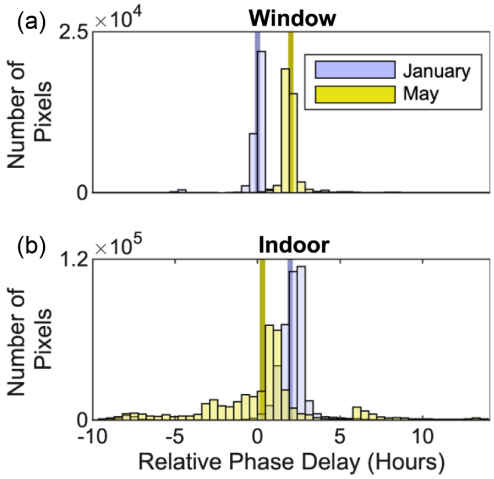

Fig. 8. Histograms showing the relative phase delay in hours of cosine-fitted pixels in the window and indoor regions. January data are shown in blue, and May data are shown in yellow. Data are aligned such that the peak in the January window data appears at 0. A negative phase delay with respect to this denotes a "phase advance." Means for each distribution are shown in the darkened bars.

and data from the May dataset are shown in yellow, with means shown by the darkened bars. The data in this figure have been aligned such that the peak of the January window data is at 0. There are many more datapoints in the "Indoor" subplot as a result of this region being markedly larger than the window section and thus featuring many more pixels. The data show different effects for the two regions. In the window region, there is a 2 h delay between the means of January and May distributions, with the May distribution being later. On the other hand, for the indoor region, there is a 1 h and 40 min delay between the January and May distributions, though here the May distribution is earlier. The data also show significantly more phase variation in the indoor region, especially during May.

In order to test if the "greening" observed in the indoor region may be attributable to the east-facing windows (see Fig. 1), we used a lightprobe setup, similar to that used in previous experiments [30,31]. By combining this setup with the circadiometer, we can create a "circadiometric lightprobe." This allowed us to capture light from a full 360 deg surround, including light entering the workspace from both the north-facing window that appeared in the January and May datasets, as well as the most visible set of east-facing windows to the right of the camera. Using the same 15 min interval capture scheme between 7:00 and 18:00, and using a 2 h interval overnight, we captured one day of lightprobe data on June 28, 2024.

Figure 9 shows an example lightprobe projected onto a sphere, and the north and large east windows are highlighted in orange and teal, respectively. We compared the L/(L + M) statistics of each of these window regions over time. Figure 9(c) shows changes in L/(L + M) over the course of the day recorded using the lightprobe setup, with the north target window shown in orange and the east target window shown in teal. The graph shows that the large east window has a consistently lower L/(L + M) statistic throughout the day (thus being "greener"), and a matched-pairs Friedman test showed that this difference was significant ($\chi^2(63) = 104.02$, $p = 0.001$).

4. DISCUSSION

The aim of this study was to collect a dataset of calibrated images taken from a typical indoor office environment across different seasons in order to assess whether some chromatic characteristics of natural environments carried over into an example mixed-illuminant indoor environment. Our data affirmed the influence of external natural scene statistics on the indoor space.

First, we showed lower L/(L + M) statistics in our May dataset compared to our January dataset (see Fig. 3), which corroborates Webster *et al.*'s finding [9] in a mixed-illuminant environment. Changes to this statistic in natural environments are associated with the "greening" of foliage in wet seasons; however, our PCA-derived segmentation that split the scene into the key "indoor" and "window" sections, allowed us to demonstrate that the lowering of L/(L + M) was due to changes in light observed in the indoor region rather than directly from the window (where foliage was directly visible), despite the fact that there were no changes in the chromaticity of the artificial illumination between the two datasets. That these differences are largely driven by the indoor region suggests that chromatic changes to the light entering the scene via the windows can markedly alter the chromatic profile of light reflected from indoor surfaces to the extent that they can reproduce the seasonal changes that occur outside, even if the windows themselves are not directly visible. We observed seasonal changes in the opposite direction for the shorter-wavelength statistics I/(L + M) and S/(L + M). Previous analysis of natural scene

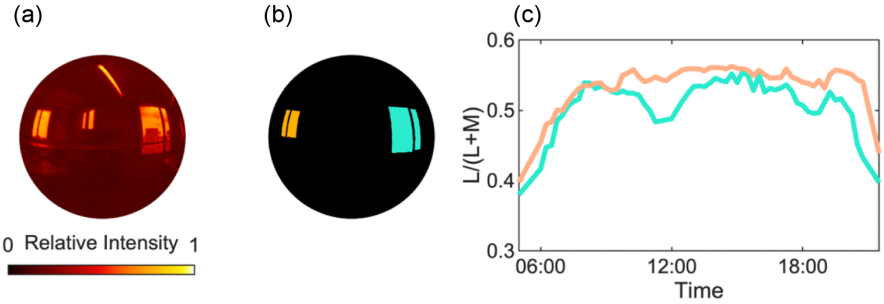

Fig. 9. Lightprobe data. (a) An example lightprobe, mapped onto a sphere, showing the north and east windows. (b) north (orange) and east (teal) target windows are highlighted. (c) Timeseries plot for the day of lightprobe data, showing the mean L/(L + M) statistics over time for the two target windows. The north window is shown in orange, and the east window is shown in teal.

statistics using principal component analysis to derive opponency channels has identified S and I opponency to L and M to explain a significant amount of variance across natural scenes [32], and our analysis demonstrates that this variance can also be observed indoors through seasonal variation.

Second, we showed that different segments of the scene, associated with higher and lower luminances, had different chromatic properties, but that this effect depended on the season (see Fig. 4). For most of the May dataset, there was an increase in the $L/(L+M)$ statistic in the higher luminance region. For the January dataset, the effect was much more varied and was most typically in the opposite direction. This suggests the regularities observed by Vincent *et al.* [12] in natural scenes can be carried over into mixed-illuminant indoor environments. Analysis provided in Fig. S5 in Supplement 1 also reveals that the bimodality observed in the January dataset was attributable to weather effects, with negative differences being observed on sunny days, and cloudy days reversing the direction of the difference.

Other than the greening of foliage, another significant way in which the outdoor environment changes across different seasons is the path the sun takes throughout the day. At the latitude of data collection, there are large differences in sun elevation in January and May, which in turn leads to significantly different chromaticities. Modeling of sun spectra at different sun elevation levels reveals that these changes in sun path could play a major role in the decrease of $L/(L+M)$ in the summer [33] (see Figs. S6–S8 in Supplement 1). The change in sun elevation had further effects on the light in the office too, such as in bright regions in the indoor region as a result of intense directional sunlight. This is exemplified by the desk-containing pixel locations that behave more similarly to the window region in the May dataset PCA, but also by the group of high-luminance datapoints that remain in the indoor classification, shown in the right column of Fig. 3, all of which occur between 06:00 and 09:00, suggesting that the early morning sun from the east-facing windows produces these bright patches. Previous experiments exploring indoor spaces using only light from windows have noted the dependence of indoor spaces on sun elevation for access to this light [34], and our findings extend these results to our mixed illuminant environments.

Weather also had a significant effect on the chromaticity not only of the window region but the indoor space too (see Figs. 6, 7, and S5). The whole image, window, and indoor region classifications all demonstrated a significant shift in chromaticity when the weather was overcast compared to when it was sunny. In all region and season combinations, overcast days were bluer and less red. For data collected on sunny days, a negative slope was observed in $L/(L+M)$ versus $S/(L+M)$ plots in January but not in May, similar to the distributions observed by Webster *et al.*, and other previous research showing blue–yellow bias in natural scenes [35]. Previous work has demonstrated how cloud coverage can affect the direction and strength of diffuse components of light [36], which in turn affects the light available to the indoor region.

We also investigated correlations between S-cone and melanopic light intensity across each region and season, as well as across weather conditions (see Fig. S9 in Supplement 1). While there were no clear weather or region effects, the strength of the correlations decreased at sunrise and sunset—particularly in May. Previous research has demonstrated an increased variance of cone excitation ratios in natural scenes in the evening [37]. The increased variance in short-wavelength light that we observe is likely partially due to changes in the directionality of illumination in the scene. Specifically, when the sun is lower in the sky, illumination is highly directional. This increases local discrepancies in the illumination of surfaces, thus decorrelating photoreceptor signals. Notably, the correlations are otherwise largely invariant. The motion-activated artificial lights are activated at around 08:30 across both datasets, though there is no clear step change observed, and the decorrelations align more with the rising and setting of the sun. This dissociation between melanopic light and S-cone signals at specific times in the diurnal cycle may provide a useful physiological signal for dawn and dusk.

We sought to specifically investigate light in the indoor region, as this represents the complex interplay of natural and artificial light, and surfaces inside the office (see Fig. S10 in Supplement 1). Correlations between luminance and different chromatic statistics within different seasons and weather conditions revealed further regularities that appear in the indoor region. Interestingly, correlations between luminance and $L/(L+M)$ were relatively stable across all conditions, but there were large differences for the short-wavelength photoreceptor correlations. On sunny days in January, luminance correlated negatively with these statistics, suggesting that the brightest pixels in the indoor region were more yellow. The strength of overcast days in January ended similarly negative to sunny days but began with a strength closer to 0, decreasing throughout the day. Meanwhile, the weather differences in May were more pronounced, with overcast days showing a persistent positive correlation, while sunny days continued to have a negative correlation. The differing effects of weather may be due to the differences in sun elevation (Fig. S6). Correlations in January may be more sensitive to the directional effect of the sun throughout the day as it stays lower in the sky, while the high path of the sun is blocked by the ceiling for most of the daytime in May. Additionally, the increased variance in the mornings of the May dataset might reflect the increased influence of natural light on the indoor region before the artificial lights turn on.

The range of phases in which light increases and decreases across different surfaces in the indoor region, as a result of the differing surface normals and locations with respect to the north and east windows, demonstrates the complex chromatic interactions that occur between the natural outdoor lighting and the large, reflective indoor surfaces, specifically as a result of directional light like the sun (see Fig. 8). By capturing a 360 deg lightprobe of the office environment, we were able to record differences in the chromaticities of the illumination entering the office from the north windows and east windows and found that the main east window—those not originally visible to the circadiometer in our January and May datasets—featured significantly lower $L/(L+M)$ values than the north windows, which may provide an explanation as to how the $L/(L+M)$ statistics of the indoor region decrease in the summer (see Fig. 9). Chromatic changes in the natural environment are very directionally sensitive and are prominently influenced by the path the sun takes and the geometric properties of objects and

surfaces from which the sun reflects. In addition to the sunlight directly entering the office, the spectra reflected by natural and built terrain around an office building change throughout the day and the year as the location of the sun and visibility of the sun due to clouds and foliage changes [38]. Because of this directional sensitivity, it is plausible that the lower $L/(L+M)$ ratio light entering the indoor office from the east was a significant determinant in changing the chromatic properties of the indoor region, while the light entering the scene from the north window was less affected by the seasonal changes typically observed between January and May. This result emphasizes the need for more mixed-illuminant datasets that quantify physiologically relevant light across the full light field using multidirectional setups.

A limitation of the data presented here is the extent to which it is generalizable to other indoor spaces due to the specificity of indoor furniture, geometry, and window locations and directions. While we note the specificity of indoor spaces and the myriad factors that affect their chromatic environments, it is significant that changes to outdoor seasonal characteristics can have such an effect on an indoor environment, and the factors that allow this to occur may be shared by many typical indoor spaces. This prompts further inquiry into different mixed-illuminant spaces, such as those with more limited access to natural light, single-direction window visibility, or different kinds of artificial lighting. This research also prompts behavioral studies, which might investigate the chromatic characteristics that lead to light-manipulating behaviors such as closing curtains or blinds and the effects this has on adaptation states.

To summarize, indoor, mixed-illuminant scenes represent complex interactions between outdoor (natural) and indoor (artificial) chromatic environments. Despite this, mixed-illuminant environments may undergo many of the same seasonal changes that naturalistic scenes experience, and this may facilitate seasonal adaptational changes that are understood to be the result of regularities in the seasonal natural environment.

Funding. Medical Research Council; Pembroke College, Oxford; Hoare Lea.

Acknowledgment. SP is supported by an Oxford-MRC Doctoral Training Partnership, Hoare Lea and Pembroke College, Oxford. We would like to thank Robert Fosbury for providing code and data for the calculation of elevation changes in sun spectra. Additionally, we would like to thank the two anonymous reviewers who provided insightful comments for our manuscript.

Disclosures. The authors declare no conflicts of interest.

Data availability. Data underlying the results presented in this paper are not publicly available at this time but may be obtained from authors upon reasonable request.

Supplemental document. See Supplement 1 for supporting content.

REFERENCES

1. J. Neitz, J. Carroll, Y. Yamauchi, *et al.*, "Color perception is mediated by a plastic neural mechanism that is adjustable in adults," Neuron **35**, 783–792 (2002).
2. B. Wozniak, J. Maule, A. Franklin, *et al.*, "Color discrimination and chromatic balance perception after adaptation to natural and color-reflected scenes," J. Vis. **23**(9), 5699 (2023).
3. A. E. Skelton, J. Maule, S. Floyd, *et al.*, "Effects of visual diet on colour discrimination and preference," Proc. R. Soc. B **291**, 20240909 (2024).
4. T. Morimoto and H. E. Smithson, "Discrimination of spectral reflectance under environmental illumination," J. Opt. Soc. Am. **35**, B244–B255 (2018).
5. A. E. Skelton, A. Franklin, and J. M. Bosten, "Color vision is aligned with natural scene statistics at 4 months of age," Dev. Sci. **26**, e13402 (2023).
6. T. Morimoto, C. Zhang, K. Fukada, *et al.*, "Spectral measurement of daylights and surface properties of natural objects in Japan," Opt. Express **30**, 3183–3204 (2022).
7. Y. Nayatani and G. Wyszecki, "Color of daylight from north sky," J. Opt. Soc. Am. **53**, 626–629 (1963).
8. G. T. Winch, M. C. Boshoff, C. J. Kok, *et al.*, "Spectroradiometric and colorimetric characteristics of daylight in the southern hemisphere: Pretoria, South Africa," J. Opt. Soc. Am. **56**, 456–464 (1966).
9. M. A. Webster, Y. Mizokami, and S. M. Webster, "Seasonal variations in the color statistics of natural images," Netw. Comput. Neural Syst. **18**, 213–233 (2007).
10. G. Tkačik, P. Garrigan, C. Ratliff, *et al.*, "Natural images from the birthplace of the human eye," PLoS One **6**, e20409 (2011).
11. L. E. Welbourne, A. B. Morland, and A. R. Wade, "Human colour perception changes between seasons," Curr. Biol. **25**, R646–R647 (2015).
12. J. Vincent, A. M. Kale, and S. L. Buck, "Luminance-dependent long-term chromatic adaptation," J. Opt. Soc. Am. **33**, A164–A169 (2016).
13. S. L. Buck and T. DeLawyer, "Dark versus bright equilibrium hues: rod and cone biases," J. Opt. Soc. Am. **31**, A75–A81 (2014).
14. N. E. Klepeis, W. C. Nelson, W. R. Ott, *et al.*, "The National Human Activity Pattern Survey (NHAPS): a resource for assessing exposure to environmental pollutants," J. Exposure Sci. Environ. Epidemiol. **11**, 231–252 (2001).
15. Y. Zeng, H. Sun, B. Lin, *et al.*, "Non-visual effects of office light environment: field evaluation, model comparison and spectral analysis," Build. Environ. **197**, 107859 (2021).
16. P. Lalande, C. M. H. Demers, F. J. Lalonde, *et al.*, "Spatial representations of melanopic light in architecture," Archit. Sci. Rev. **64**, 522–533 (2021).
17. J. Hraška, "Nonvisual aspects of daylight in the built environment," IOP Conf. Ser. **1252**, 012063 (2022).
18. O. Stefani and C. Cajochen, "Should we re-think regulations and standards for lighting at workplaces? A practice review on existing lighting recommendations," Front Psychiatry **12**, 652161 (2021).
19. R. Zhang, C. Campanella, S. Aristizabal, *et al.*, "Impacts of dynamic LED lighting on the well-being and experience of office occupants," Int. J. Environ. Res. Public Health **17**, 7217 (2020).
20. F. S. Webler, M. Spitschan, R. G. Foster, *et al.*, "What is the 'spectral diet' of humans?" Curr. Opin. Behav Sci. **30**, 80–86 (2019).
21. CIE, "CIE S 026/E:2018: CIE System for Metrology of Optical Radiation for ipRGC-Influenced Responses to Light," (2018).
22. A. Stockman, "Macleod & Boynton (1979) 2-deg chromaticity coordinates based on the Stockman & Sharpe (2000) cone fundamentals," http://www.cvrl.org/database/text/ccs/mb2.htm.
23. A. B. Watson and J. I. Yellott, "A unified formula for light-adapted pupil size," J. Vis. **12**(10), 12 (2012).
24. M. Spitschan, "Photoreceptor inputs to pupil control," J. Vis. **19**(9), 5 (2019).
25. R. F. Hess and K. Nordby, "Spatial and temporal properties of human rod vision in the achromat," J. Physiol. **371**, 387–406 (1986).
26. M. Aguilar and W. S. Stiles, "Saturation of the rod mechanism of the retina at light levels of stimulation," Opt. Acta **1**, 59–65 (1954).
27. A. G. Shapiro, J. Pokorny, and V. C. Smith, "Cone-rod receptor spaces with illustrations that use CRT phosphor and light-emitting-diode spectra," J. Opt. Soc. Am. A **13**, 2319–2328 (1996).
28. "Time and Date," Oxford England, https://www.timeanddate.com/sun/uk/oxford.
29. M. Spitschan, S. Jain, D. H. Brainard, *et al.*, "Opponent melanopsin and S-cone signals in the human pupillary light response," Proc. Natl. Acad. Sci. USA **111**, 15568–15572 (2014).

30. T. Morimoto, S. Kishigami, J. M. M. Linhares, *et al.*, "Hyperspectral environment illumination maps: characterising directional spectral variation in natural environments," Opt. Express **27**, 32277–32293 (2019).
31. L. Shiwen, L. Steele, C. A. L. Dahlsjö, *et al.*, "Hyperspectral characterisation of natural illumination in woodland forest environments," bioRxiv (2021).
32. P. A. Barrionuevo and D. Cao, "Contributions of rhodopsin, cone opsins and melanopsin to postreceptoral pathways inferred from natural scene statistics," J. Opt. Soc. Am. A **31**, A131–A139 (2014).
33. H. E. Smithson, P. S. Anderson, G. Dinkova-Bruun, *et al.*, "Color-coordinate system from a 13th-century account of rainbows," J. Opt. Soc. Am. A **31**, A341–A349 (2014).
34. M. Englezhou and A. Michael, "Investigation of the daylight spectrum in an indoor environment using the CIE S 026 melanopic metrics," Light. Res. Technol. **55**, 690–711 (2023).
35. M. A. Webster and J. D. Mollon, "Adaptation and the color statistics of natural scenes," Vis. Res. **37**, 3283–3298 (1997).
36. C. Yu, S. Pont, R. Pastilha, *et al.*, "Unveiling the temporal dynamics of diurnal and crepuscular illumination," J. Vis. **24**(10), 1211 (2024).
37. D. H. Foster, K. Amaro, and S. M. C. Nascimento, "Time-lapse ratios of cone excitations in natural scenes," Vis. Res. **120**, 45–60 (2016).
38. C. Yu, M. Wijntjes, E. Eisemann, *et al.*, "Quantifying the spatial, temporal, angular and spectral structure of effective daylight in perceptually meaningful ways," Opt. Express **31**, 8953–8974 (2023).